RSC Advances

PAPER

View Article Online
View Journal | View Issue

Cite this: *RSC Adv.*, 2019, **9**, 40546

Synthesis of Fe_3O_4@PVBC–TMT nanoparticles for the efficient removal of heavy metals ions

Zhiming Chen, * Jiaojiao Song, Qingpeng Zhu, Zhiguo Li and Renchun Yang

Received 3rd October 2019
Accepted 28th November 2019

DOI: 10.1039/c9ra08037f

rsc.li/rsc-advances

Core–shell magnetic Fe_3O_4@PVBC–TMT (Fe_3O_4@polyvinylbenzyl chloride–trithiocyanuric acid) nanoparticles containing trithiocyanuric acid groups were fabricated and employed for the fast removal of heavy metals from an aquatic environment. The morphology, structure and properties of Fe_3O_4@PVBC–TMT nanoparticles were characterized by a series of modern analytical tools. The adsorption behavior of the Fe_3O_4@PVBC–TMT nanoparticles for heavy metals ions in aqueous solutions was investigated by batch experiments. The maximum removal capacities of the Fe_3O_4@PVBC–TMT nanoparticles toward Mn^{2+}, Ni^{2+}, Cu^{2+}, Cd^{2+} and Pb^{2+} ions were 127.4, 146.6, 180.5, 311.5, and 528.8 mg g^{-1}, respectively. Importantly, it is found that Pb^{2+} ions can be completely and quickly removed by the Fe_3O_4@PVBC–TMT nanoparticles. The equilibrium was established within 6 min, and the removal efficiencies were found to be 99.9%, 99.8% and 99.5% for Pb^{2+} ions at the initial concentrations of 100 mg L^{-1}, 200 mg L^{-1} and 300 mg L^{-1}, respectively. It is hoped that the core–shell magnetic Fe_3O_4@PVBC–TMT nanoparticles may find application in wastewater treatment.

Introduction

With the rapid growth of global industrialization, uncontrolled release of heavy metals into water has been a serious environmental problem for human health since heavy metal ions are toxic and tend to accumulate in living organisms.[1] So, many efforts have been devoted to explore different technologies to prevent further heavy metal discharge and contamination. Thus far, a wide range of methods including adsorption, chemical precipitation, membrane filtration, solvent extraction, ion exchange and electrochemical technologies, have been developed to remove hazardous heavy metal ions from wastewater, in which adsorption has increasingly received more attention as it is simple and effective for the treatment of heavy metal containing water.[2–6] Thanks to many years of efforts from various groups, different kinds of adsorbents for various applications have been commercialized or are developing.[7–15] However, the benefits of this technique are offset by the additional separation step to remove suspended adsorbents from the wastewater treatment system.

Nowadays, Fe_3O_4 based magnetic nanosorbents have attracted considerable attention due to their convenient separation and manipulation based on their unique magnetic properties.[16,17] It has been widely recognized that removal capacities of adsorbents are controlled in part by the number of available functional groups used for binding metal ions.[18] In general, an excellent magnetic adsorbent possesses not only the high performance in adsorption, but also has a high stability in various chemical and physical environments such as acid or base media. Polymers are known for the outstanding stability in extreme conditions and a platform for chelating groups, and can be used in various circumstances. So, a wide variety of magnetic polymers, including dithiocarbamate–Fe_3O_4@-poly(vinyl amine) (DTC–Fe_3O_4@PVAM), Fe_3O_4–polydopamine, Fe_3O_4@organodisulfide polymer (Fe_3O_4@PTMT), Fe_3O_4/chitosan, Fe_3O_4/polyaniline/MnO_2 (Fe_3O_4/PANI/MnO_2), poly(methyl methacrylate)-grafted alginate/Fe_3O_4 (PMMA-gft-Alg/Fe_3O_4), polyacrylic acid/graphene oxide/Fe_3O_4 (PAA/GO/Fe_3O_4), Fe_3O_4/methacryloxy propyl trimethoxyl silane/polyacrylic acid (Fe_3O_4/MPTMS/PAA), polyethyleneimine–Fe_3O_4 (PEI–Fe_3O_4), and so on, have been successfully synthesized for environmental purposes.[19–35] Despite the growing numbers of magnetic polymers, Fe_3O_4/polystyrene (Fe_3O_4/PS) based nanosorbents are difficult to obtain. This was mainly because the polystyrene shell were hydrophobic and chemically inert, which is obviously disadvantageous for the further functionalized with chelating groups. Therefore, the development of strategies for the fabrication of magnetic Fe_3O_4/PS nanoparticles modified with organic functional groups is seriously considered.

Bearing this in mind, we synthesized core–shell magnetic Fe_3O_4@PVBC–TMT nanoparticles for the fast removal of heavy metals from aquatic environment (Fig. 1), which involves tri-step procedures: (1) fabrication of Fe_3O_4 nanoparticles serving as magnetic cores; (2) coating the Fe_3O_4 cores with a layer of PVBC to form core–shell structured Fe_3O_4@PVBC nanoparticles *via* a free-radical polymerization process; (3) functionalizing the Fe_3O_4@PVBC nanoparticles with trithiocyanuric acid groups by

School of Biological and Chemical Engineering, Anhui Polytechnic University, Wuhu 241000, China. E-mail: zmchen@ahpu.edu.cn

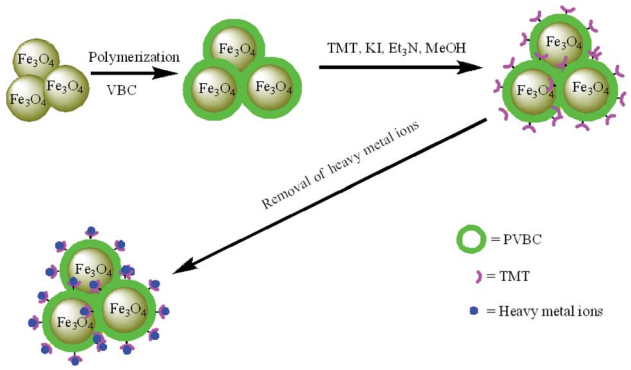

Fig. 1 Schematic representation the fabrication procedure of Fe_3O_4@PVBC–TMT nanoparticles for fast removal of heavy metal ions.

reacting with trithiocyanuric acid in the present of potassium iodide and triethylamine. Due to the magnetic nature of Fe_3O_4 cores and the functionalized organosulfide groups of PVBC–TMT shells, the Fe_3O_4@PVBC–TMT nanoparticles were expected to be a valid adsorbent for the removal of heavy metals from aquatic environment. The performance of Fe_3O_4@PVBC–TMT nanoparticles was demonstrated by batch adsorption experiments. It is believed that the results of the present investigation may provide a versatile approach for designing and fabricating magnetic adsorbent for effluent treatment.

Experimental

Materials

Ferric triacetylacetonate ($Fe(acac)_3$), 99.9%, trithiocyanuric acid (TMT), potassium persulfate (KPS), potassium iodide (KI), oleic acid (90%), oleylamine (>70%), phenyl ether, dodecanol and triethylamine were purchased from Aladdin Chemical Co. Ltd. (Shanghai, China). Vinylbenzyl chloride (VBC) was purchased from J&K Scientific Ltd. (China) and was purified by vacuum distillation. All other chemicals and reagents were analytical grade, purchased from Sinopharm Chemical Reagent Co., Ltd. (Shanghai, China), and used without further purification. Deionized water was used throughout.

Synthesis of Fe_3O_4@PVBC–TMT nanoparticles

Fe_3O_4@PVBC nanoparticles were synthesized by our method described previously.[36] In a typical procedure, 800 mg Fe_3O_4@PVBC nanoparticles, 1880 mg TMT and 560 mg KI were dispersed in 50 mL methanol to form a colloidal solution by sonication. After addition of 10 mL of triethylamine, the mixed system was transferred into a flask, and refluxed under N_2 atmosphere for 24 h. Subsequently, the system was allowed to cool to room temperature naturally. The as-obtained precipitate was collected, washed with methanol and water 3 times, and dried in a vacuum oven at 70 °C for 8 h.

Adsorption procedures of heavy metal ions

Adsorption capacities were performed by mixing 10 mg of Fe_3O_4@PVBC–TMT nanoparticles with 10 mL of $Pb(NO_3)_2$, $Cd(NO_3)_2$, $MnSO_4$, $NiSO_4$, and $CuSO_4$ solutions at initial metal ions concentration of 1000 mg L^{-1}, respectively. The mixture was left in a shaker operating at 200 rpm for 1 h. After the reaction, the adsorbents were separated by a permanent magnet. The heavy metal ions concentrations were measured by using an inductively coupled plasma spectrometer (Optima 5300DV-ICP, PerkinElmer). The adsorption capacities of Fe_3O_4@PVBC–TMT nanoparticles were calculated from mass balance. Adsorption experiments of Pb^{2+} were performed to determine the adsorption equilibrium time at different concentrations of $Pb(NO_3)_2$ solution. The initial Pb^{2+} concentrations were set from 100 to 600 mg L^{-1}. The adsorption processes were conducted in a shaker at 200 rpm for 1–50 min. The effect of pH (2.0–7.0 adjusted by 0.1 M NaOH and HNO_3) of Pb^{2+} was investigated. The regeneration of the Fe_3O_4@PVBC–TMT nanoparticles were treated with 0.2 M EDTA-2Na for 2 h and then washed with deionized water for 3 times. The Pb^{2+} concentration at various contact time was analyzed using an inductively coupled plasma spectrometer.

Characterizations

Powder X-ray diffraction (XRD) pattern was collected on a Bruker D8 Advance diffractometer. Scanning electron microscopy (SEM) image was recorded with a Hitachi S-4800 field-emission scanning electron microscope. Transmission electron microscopy (TEM) images were observed using a JEM-2010 high-resolution transmission electron microscope. Fourier transform infrared spectroscopy (FT-IR) spectra were measured on a Nicolet 5700 FT-IR spectrophotometer. X-ray photoelectron spectroscopy (XPS) was collected on an ESCALAB 250Xi by Thermo-VG Scientific. Magnetic measurement was carried out on a superconducting quantum interference device (Quantum Design MPMS XL-7).

Results and discussion

The morphologies of the as-prepared Fe_3O_4@PVBC–TMT samples were visualized by SEM and TEM. Fig. 2a shows a typical SEM image of the product and reveals that the Fe_3O_4@PVBC–TMT nanoparticles exhibit an obvious spherical morphology with a diameter of 20–50 nm. The dark/light contrast clearly observed in TEM image (Fig. 2b) suggests a different phase composition and indicates core–shell structure of Fe_3O_4@PVBC–TMT nanoparticles. Careful observation shows that the Fe_3O_4 cores are encapsulated in polymer shells and that there is no obvious void between the core and the shell. The selected area electron diffraction (SAED) pattern from Fe_3O_4@PVBC–TMT nanoparticles shows diffraction rings of Fe_3O_4 with a face-centered cubic (fcc) structure (Fig. 2c). Fig. 2d shows a high resolution TEM (HRTEM) image of Fe_3O_4@PVBC–TMT nanoparticles, which illustrates the formation of Fe_3O_4@PVBC–TMT core–shell nanostructures. The periodic fringe spacing calculated from the inside nanoparticle was 0.25 nm, fitting well with the (311) planes of fcc Fe_3O_4 structure. More importantly, an amorphous polymer layers are observed outside of the Fe_3O_4 nanoparticles.

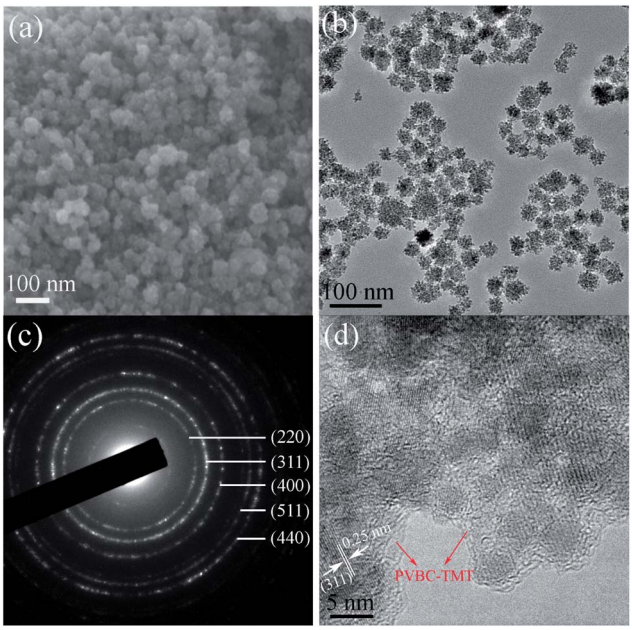

Fig. 2 (a) SEM, (b) TEM, (c) SAED and (d) HRTEM images of Fe_3O_4@PVBC–TMT nanoparticles.

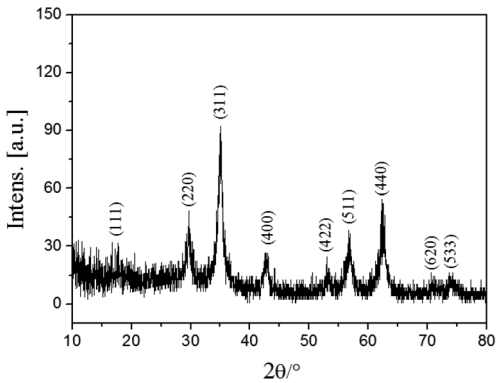

Fig. 3 XRD pattern of Fe_3O_4@PVBC–TMT nanoparticles.

Fig. 3 displays a typical XRD pattern of the as-synthesized Fe_3O_4@PVBC–TMT nanoparticles. All diffraction peaks of the Fe_3O_4@PVBC–TMT nanoparticles can be readily indexed to fcc Fe_3O_4 with lattice constants a = 8.396 Å, which are in good agreement with the literature values (JCPDS no. 77-1545). The mean grain sizes of Fe_3O_4 crystals estimated from the Debye–Scherrer equation based on the five strongest peaks (220, 311, 400, 511, and 440) was calculated to be 15.2 nm.

The surface information of the magnetic nanoparticles contains different functions was studied by FT-IR spectroscopy (Fig. 4). As shown in Fig. 4a, the strong peak at 578 cm^{-1} is attributed to the characteristic band of Fe–O vibration. The peaks at 2923, 2847, 1633, 1516, 1458, 1416, 1062 and 823 cm^{-1} were associated with existent abundant of benzene ring and methylene in the polymer main chain. The vibration bands at 1268 and 645 cm^{-1} were assigned to stretching vibrations of CH_2–Cl.[37] These results reveal that a large amount of –CH_2Cl

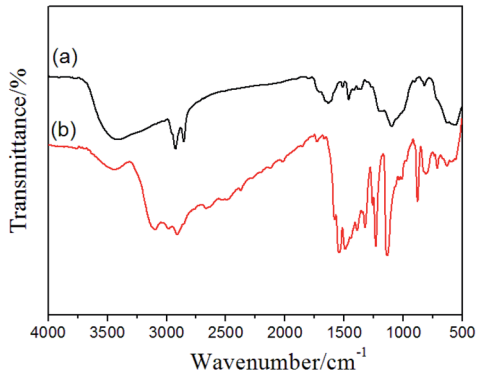

Fig. 4 FT-IR spectra of (a) Fe_3O_4@PVBC nanoparticles, and (b) Fe_3O_4@PVBC–TMT nanoparticles.

functional groups were bonded to the polymer shell in the Fe_3O_4@PVBC nanoparticles, which made possible the covalent binding of functional molecules (*e.g.* trithiocyanuric acid) for the adsorption of heavy metals ions. In order to obtain the magnetic adsorbents, the Fe_3O_4@PVBC nanoparticles were reacted with trithiocyanuric acid in the presence of triethylamine and KI. It is observed that the peaks in the range 2899–3136 cm^{-1} for N–H stretching in triazine groups and absorption bands in the range of 1000–1600 cm^{-1} (stretching modes of C=S and C–N heterocycles) appeared (Fig. 4b),[38,39] indicating that trithiocyanuric acid was covalently bonded to the polymer shell of Fe_3O_4@PVBC nanoparticles.

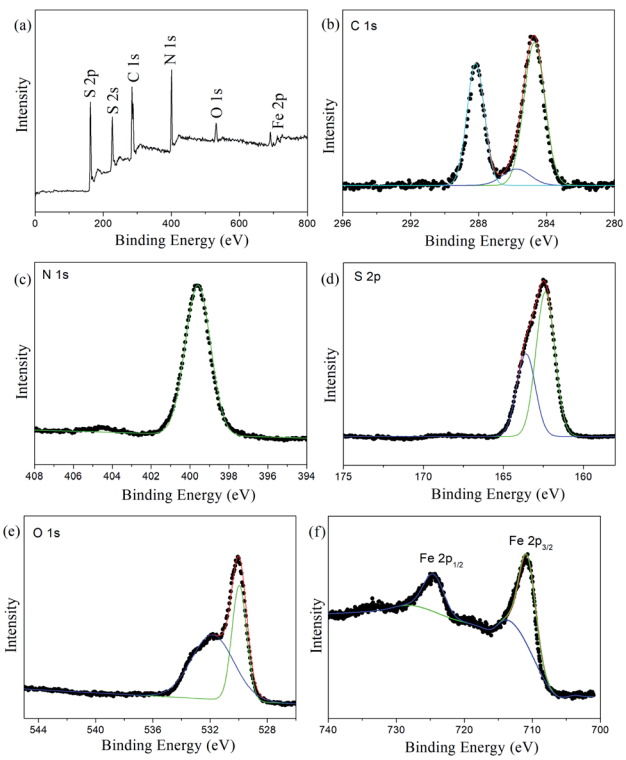

Fig. 5 (a) Full-scan, (b) C 1s, (c) N 1s, (d) S 2p, (e) O 1s and (f) Fe 2p XPS spectra of Fe_3O_4@PVBC–TMT nanoparticles.

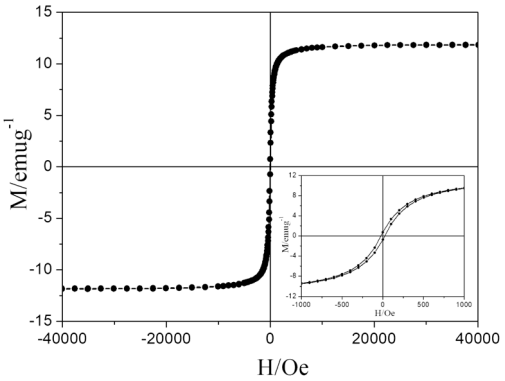

Fig. 6 The room-temperature magnetic hysteresis loop of Fe_3O_4@PVBC–TMT nanoparticles.

Fig. 5 a shows the full-scan X-ray photoelectron spectroscopy (XPS) spectrum of Fe_3O_4@PVBC–TMT nanoparticles, which is mainly composed of C, N, S, O and Fe elements. The asymmetric C 1s peak is decomposed into three peaks at 284.6, 285.6 and 288.0 eV (Fig. 5b). The peak at 284.6 eV can be ascribed to the graphitic carbon (C–C and C=C). The peaks centered at about 285.6 and 288.0 eV are typically attributed to the C–S bonded in the triazine ring and the sp^2 hybrid C atoms bonded to N-containing skeleton rings (N–C=N), respectively.[40,41] The N 1s peak is located at 399.6 eV (Fig. 5c), which could be attributed to the N atoms bonded to carbon atoms in triazine rings.[42] The S 2p peaks were observed at 162.4 and 163.6 eV (Fig. 5d), which could be attributed to S $2P_{3/2}$ and S $2P_{1/2}$ binding energies for C–S bonds, respectively.[43] The O spectrum in Fig. 5e confirms that a sharp peak originated from the oxygen in Fe_3O_4 (523.0 eV) and a shoulder peak centered at 531.7 eV, which can be assigned to the surface traps.[44] It is observed that the Fe $2p_{3/2}$ and Fe $2p_{1/2}$ peaks are found to be located at 710.7 and 724.5 eV (Fig. 5d), respectively, which is consistent with the oxidation state of Fe in Fe_3O_4.[44] These results demonstrate that the magnetic composites are Fe_3O_4@PVBC–TMT nanoparticles, which are consistent with the FT-IR spectra.

Fig. 6 shows the isothermal magnetization of the Fe_3O_4@PVBC–TMT nanoparticles. It could be observed that Fe_3O_4@PVBC–TMT nanoparticles show ferromagnetic behavior with the magnetic saturation value of 11.9 emu g^{-1}. The decrease in magnetic saturation of Fe_3O_4@PVBC–TMT nanoparticles in comparison with Fe_3O_4 might be attributed to the increased mass of the nonmagnetic PVBC–TMT on the surface of the magnetic nanoparticles. The magnetic separability of the Fe_3O_4@PVBC–TMT nanoparticles was tested in aqueous solution by placing a magnet near the glass bottle. All the black particles were absorbed on the wall of the vial within 30 s, demonstrating directly that the Fe_3O_4@PVBC–TMT nanoparticles possess magnetic properties. This is an essential factor in the separation and reuse of magnetic Fe_3O_4@PVBC–TMT nanoparticles for practical applications.

To show the versatility of the Fe_3O_4@PVBC–TMT nanoparticles, the extraction of Mn^{2+}, Ni^{2+}, Cu^{2+}, Cd^{2+} and Pb^{2+} ions from aqueous solution was tested at the concentration of 1000 mg L^{-1}. The supernatant solution was collected for quantitative element analysis by ICP. Fig. 7 shows the adsorption capacities to which by using Fe_3O_4@PVBC–TMT nanoparticles as the adsorbents. The maximum adsorption capacities of Fe_3O_4@PVBC–TMT nanoparticles were 127.4 mg g^{-1} for Mn^{2+}, 146.6 mg g^{-1} for Ni^{2+}, 180.5 mg g^{-1} for Cu^{2+}, 311.5 mg g^{-1} for Cd^{2+} and 528.8 mg g^{-1} for Pb^{2+} ions, respectively. The order of capacity of Fe_3O_4@PVBC–TMT nanoparticles is Pb^{2+} > Cd^{2+} > Cu^{2+} > Ni^{2+} > Mn^{2+}. The difference in the behavior of these metal ions may be related to the strength of their coordination complexes with Fe_3O_4@PVBC–TMT nanoparticles.

Fig. 8 shows effects of solution pH on Pb^{2+} adsorption by Fe_3O_4@PVBC–TMT nanoparticles. It is found that the pH value plays an important role in Pb^{2+} adsorption. The absorption capacity was relative low when the pH value is lower than 4. When the pH value increased to 5, the absorption capacity increased dramatically. The reason for this phenomenon may be related to the protonation. When the pH is relative low, the concentrated H^+ could protonate the functional groups (–SH) on the surface of Fe_3O_4@PVBC–TMT nanoparticles. The electrostatic repulsion between –SH groups and Pb^{2+} will result in the low absorption capacity.

Rapid interaction of the pollutants to be separated with the adsorbent is desirable and beneficial for practical adsorption

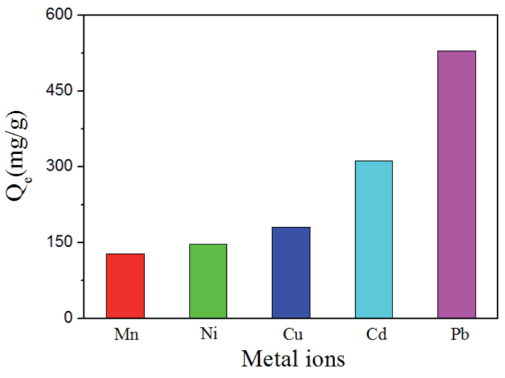

Fig. 7 The adsorption capacities of the Fe_3O_4@PVBC–TMT nanoparticles toward Mn^{2+}, Ni^{2+}, Cu^{2+}, Cd^{2+} and Pb^{2+} ions.

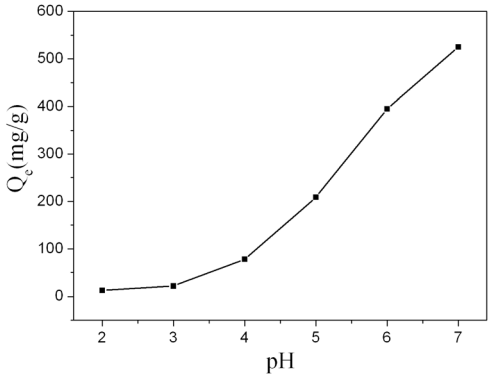

Fig. 8 Effects of solution pH on Pb^{2+} adsorption by Fe_3O_4@PVBC–TMT nanoparticles.

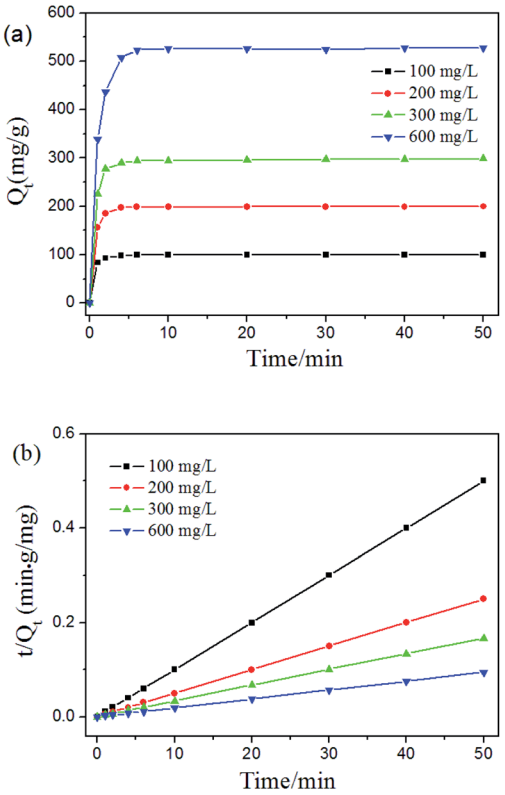

Fig. 9 (a) Equilibrium isotherms and (b) fitting curve of pseudo-second-order for Pb^{2+} ion by Fe_3O_4@PVBC–TMT nanoparticles at the initial concentrations of 100, 200, 300 and 600 mg L^{-1}.

applications. Understanding the adsorption behavior of pollutants is of great importance for the removal heavy metal ions from aqueous environments. Considering the excellent performance in the Pb^{2+} removal capacity, we studied the kinetic behavior of the adsorption process by adding 10 mg of dried Fe_3O_4@PVBC–TMT nanoparticles into 10.0 mL Pb^{2+} ion aqueous solutions. It can be observed from Fig. 9a that Pb^{2+} ion uptake on Fe_3O_4@PVBC–TMT nanoparticles was a fast process. The amount of adsorption increased rapidly in the first 4 min, contributing to 94.6% of the ultimate adsorption amount, and then augmented slowly and approached the adsorption equilibrium in about 6 min. The removal efficiencies were found to be 99.9%, 99.8% and 99.5% for Pb^{2+} ion at the initial concentrations of 100 mg L^{-1}, 200 mg L^{-1} and 300 mg L^{-1}, respectively. The total amount of Pb^{2+} ion adsorbed increased with the increasing initial Pb^{2+} ion concentrations. This is because the higher initial Pb^{2+} concentration provides higher driving force for the ions from the solution to the Fe_3O_4@PVBC–TMT nanoparticles, resulting in more collisions between Pb^{2+} ion and active sites on the Fe_3O_4@PVBC–TMT nanoparticles.

To determine the rate-controlling and mass transfer mechanism, adsorptive data were correlated to linear forms of the pseudo-first-order rate model

$$\ln(q_e - q_t) = \ln q_e - k_1 t \quad (1)$$

and the pseudo-second-order rate equation

$$\frac{t}{q_t} = \frac{1}{k_2 q_e^2} + \frac{t}{q_e} \quad (2)$$

where q_e and q_t (mg g^{-1}) are the amounts of Pb^{2+} ion adsorbed at equilibrium and at different intervals, respectively. k_1 (min^{-1}) and k_2 (g mg^{-1} min^{-1}) are the pseudo-first- and pseudo-second-order rate constants. The values of the rate constants are determined from the intercepts of the curves and are given in Table 1. The correlation coefficient (R^2) for the pseudo-second-order adsorption model has high value for Pb^{2+} ion. The maximum adsorption capacity of Fe_3O_4@PVBC–TMT nanoparticles toward Pb^{2+} ions was calculated to be 529.1 mg g^{-1} (Fig. 9b), which is higher than the reported magnetic sorbents.[22,23] The maximum adsorption capacity of Fe_3O_4@PVBC–TMT nanoparticles is consistent with the experimental data, indicating that the present sorption system follows predominantly the pseudo-second-order rate model and the overall process appears to be controlled by chemisorptions.[45,46]

The reusability of the Fe_3O_4@PVBC–TMT nanoparticles was determined by adsorption of Pb^{2+} as a reported literature.[22] The regeneration process of the absorbents was performed by using EDTA-2Na solution as desorbent after adsorption process. The adsorption–desorption cycles were repeated using the same method. As the number of regeneration increased, the re-adsorption amounts of Pb^{2+} decreased drastic. The re-adsorption amounts of Pb^{2+} in the first and second regeneration were found to be 125.1 mg g^{-1} and 58.3 mg g^{-1}, respectively. The decrease of re-adsorption amount is mainly ascribed to the leakage of PVBC–TMT from magnetic absorbents upon desorption process.

Conclusions

In summary, we presented a facile and practical approach to synthesis core–shell magnetic Fe_3O_4@PVBC–TMT nanoparticles. TEM images confirmed the core–shell structure of the

Table 1 Parameters of removal kinetics and adsorption capacities of Fe_3O_4@PVBC–TMT nanoparticles toward Pb^{2+} ion

	Pseudo-first-order equation			Pseudo-second-order equation		
Initial concentration (mg L^{-1})	q_e (mg g^{-1})	K_1 (min^{-1})	R^2	q_e (mg g^{-1})	K_2 (g mg^{-1} min^{-1})	R^2
100	99.4	1.7890	0.9686	100.1	0.1392	1.0000
200	198.8	1.4882	0.9686	200.0	0.0499	1.0000
300	295.9	1.4245	0.9851	299.4	0.0209	0.9999
600	523.7	0.9856	0.9764	529.1	0.0085	0.9999

product. FT-IR and XPS spectra indicated that the Fe_3O_4@PVBC–TMT nanoparticles were functionalized with trithiocyanuric acid groups. Combining the merits of easy separation of the Fe_3O_4 core and trithiocyanuric acid groups of polymer shell, the Fe_3O_4@PVBC–TMT nanoparticles has been demonstrated to be a valid adsorbent for the fast removal of heavy metals from aquatic environment. Batch adsorption experiments showed that the maximum removal capacities of the Fe_3O_4@PVBC–TMT nanoparticles toward Mn^{2+}, Ni^{2+}, Cu^{2+}, Cd^{2+} and Pb^{2+} ions were 127.4, 146.6, 180.5, 311.5, and 528.8 mg g^{-1}, respectively. Due to the strong interactions between the functionalized groups and heavy metal ions, an ultrafast removal process (94.6% within 4 min) was observed in Pb^{2+} ion aqueous solutions with a high concentration. The removal efficiencies were found to be 99.9%, 99.8% and 99.5% for Pb^{2+} ion at the initial concentrations of 100 mg L^{-1}, 200 mg L^{-1} and 300 mg L^{-1}, respectively. This investigation showed that the present core–shell magnetic Fe_3O_4@PVBC–TMT nanoparticles have a potential application in wastewater treatment and environmental protection.

Conflicts of interest

There are no conflicts to declare.

Acknowledgements

This work is supported by the National Natural Science Foundation of China (21471002 and 51572004) and the Young and Middle-Aged Talent Program of Anhui Polytechnic University (2016BJRC001).

Notes and references

1 D. W. Wang, Y. Li, G. L. Puma, P. Lianos, C. Wang and P. F. Wang, *J. Hazard. Mater.*, 2017, **323**, 681–689.
2 A. Z. M. Badruddoza, Z. B. Z. Shawon, T. W. J. Daniel, K. Hidajat and M. S. Uddin, *Carbohydr. Polym.*, 2013, **91**, 322–332.
3 J. X. Yu, L. Y. Wang, R. A. Chi, Y. F. Zhang, Z. G. Xu and J. Guo, *Appl. Surf. Sci.*, 2013, **268**, 163–170.
4 L. M. Zhou, Y. P. Wang, Z. R. Liu and Q. W. Huang, *J. Hazard. Mater.*, 2009, **161**, 995–1002.
5 M. Xu, Y. S. Zhang, Z. M. Zhang, Y. O. Shen, M. J. Zhao and G. T. Pan, *Chem. Eng. J.*, 2011, **168**, 737–745.
6 Q. Q. Ou, L. Zhou, S. G. Zhao, H. J. Geng, J. J. Hao, Y. Y. Xu, H. L. Chen and X. G. Chen, *Chem. Eng. J.*, 2012, **180**, 121–127.
7 H. H. Zeng, L. Wang, D. Zhang, P. Yan, J. Nie, V. K. Sharma and C. Y. Wang, *Chem. Eng. J.*, 2019, **358**, 253–263.
8 M. Sharma, M. Joshi, S. Nigam, S. Shree, D. K. Avasthi, R. Adelung, S. K. Srivastava and Y. K. Mishra, *Chem. Eng. J.*, 2019, **358**, 540–551.
9 N. Blagojev, D. Kukić, V. Vasić, M. Šćiban, J. Prodanović and O. Bera, *J. Hazard. Mater.*, 2019, **363**, 366–375.
10 Y. Z. Wu, Y. J. Ma, G. H. Xu, T. Y. Xia, W. X. Liu, Z. Z. Dong, Q. Y. Yuan, C. Zhang and Q. Hu, *J. Mater. Sci.*, 2019, **54**, 2093–2101.
11 S. B. Wang and Y. L. Peng, *Chem. Eng. J.*, 2010, **156**, 11–24.
12 J. Goel, K. Kadirvelu, C. Rajagopal and V. K. Garg, *J. Hazard. Mater.*, 2005, **125**, 211–220.
13 C. J. Madadrang, H. Y. Kim, G. H. Gao, N. Wang, J. Zhu, H. Feng, M. Gorring, M. L. Kasner and S. F. Hou, *ACS Appl. Mater. Interfaces*, 2012, **4**, 1186–1193.
14 Z. X. Wu and D. Y. Zhao, *Chem. Commun.*, 2011, **47**, 3332–3338.
15 A. Walcarius and L. Mercier, *J. Mater. Chem.*, 2010, **20**, 4478–4511.
16 Z. Y. Zhang and J. L. Kong, *J. Hazard. Mater.*, 2011, **193**, 325–329.
17 W. J. Zhang, X. H. Shi, Y. X. Zhang, W. Gu, B. Y. Li and Y. Z. Xian, *J. Mater. Chem. A*, 2013, **1**, 1745–1753.
18 M. Monier, *Int. J. Biol. Macromol.*, 2012, **50**, 773–781.
19 X. Wang, S. Y. Jing, Z. S. Hou, Y. Y. Liu, X. M. Qiu, Y. S. Liu and Y. B. Ten, *J. Mater. Sci.*, 2018, **53**, 15009–15024.
20 E. Yavuz, S. Tokalioglu and S. Patat, *Food Chem.*, 2018, **263**, 232–239.
21 Q. L. Fang, S. X. Duan, J. F. Zhang, J. X. Li and K. C. F. Leung, *J. Mater. Chem. A*, 2017, **5**, 2947–2958.
22 X. Huang, J. Y. Yang, J. K. Wang, J. T. Bi, C. Xie and H. X. Hao, *Chemosphere*, 2018, **206**, 513–521.
23 H. L. Fan, S. F. Zhou, W. Z. Jiao, G. S. Qi and Y. Z. Liu, *Carbohydr. Polym.*, 2017, **174**, 119–1200.
24 J. Zhang, J. Han, M. G. Wang and R. Guo, *J. Mater. Chem. A*, 2017, **5**, 4058–4066.
25 A. Mittal, R. Ahmad and I. Hasan, *Desalin. Water Treat.*, 2016, **57**, 19820–19833.
26 X. Y. Guan, S. X. Yan, Q. Zeng, Z. Xu, Y. Chen and H. J. Fan, *Fibers Polym.*, 2016, **17**, 1131–1139.
27 S. Lapwanit, T. Trakulsujaritchok and P. N. Nongkhai, *Chem. Eng. J.*, 2016, **289**, 286–295.
28 H. N. M. E. Mahmud, A. K. O. Huq and R. B. Yahya, *RSC Adv.*, 2016, **6**, 14778–14791.
29 S. Venkateswarlu and M. Yoon, *ACS Appl. Mater. Interfaces*, 2015, **7**, 25362–25372.
30 O. V. Kharissova, H. V. R. Dias and B. I. Kharisov, *RSC Adv.*, 2015, **5**, 6695–6719.
31 X. B. Fang, Z. Q. Fang, P. K. E. Tsang, W. Cheng, X. M. Yan and L. C. Zheng, *Appl. Surf. Sci.*, 2014, **314**, 655–662.
32 R. Hua and Z. K. Li, *Chem. Eng. J.*, 2014, **249**, 189–200.
33 F. Ge, M. M. Li, H. Ye and B. X. Zhao, *J. Hazard. Mater.*, 2012, **211–212**, 366–372.
34 K. Zargoosh, H. Abedini, A. Abdolmaleki and M. R. Molavian, *Ind. Eng. Chem. Res.*, 2013, **52**, 14944–14954.
35 Y. Pang, G. M. Zeng, L. Tang, Y. Zhang, Y. Y. Liu, X. X. Lei, Z. Li, J. C. Zhang, Z. F. Liu and Y. Q. Xiong, *Chem. Eng. J.*, 2011, **175**, 222–227.
36 Z. M. Chen, L. L. Liu and R. C. Yang, *RSC Adv.*, 2017, **7**, 35169–35174.
37 W. T. Lu, Z. G. Shao, G. Zhang, Y. Zhao and B. L. Yi, *J. Power Sources*, 2014, **248**, 905–914.
38 J. D. Hong, X. Y. Xia, Y. S. Wang and R. Xu, *J. Mater. Chem.*, 2012, **22**, 15006–15012.
39 D. Ko, J. Lee, H. A. Patel, M. H. Jakobsen, Y. Hwang, C. T. Yavuz, H. C. B. Hansen and H. R. Andersen, *J. Hazard. Mater.*, 2017, **332**, 140–148.

40 H. L. Dou, S. H. Zheng and Y. P. Zhang, *RSC Adv.*, 2018, **8**, 7558–7568.
41 T. Sirtl, M. Lischka, J. Eichhorn, A. Rastgoo-Lahrood, T. Strunskus, W. M. Heckl and M. Lackinger, *J. Phys. Chem. C*, 2014, **118**, 3590–3598.
42 C. Xiong, S. X. Wang, L. B. Zhang, Y. Li, Y. Zhou and J. H. Peng, *J. Mol. Liq.*, 2018, **254**, 340–348.
43 R. S. Vishwanath and S. Kandaiah, *Int. J. Hydrogen Energy*, 2016, **41**, 8829–8838.
44 Y. Tian, B. B. Yu, X. Li and K. Li, *J. Mater. Chem.*, 2011, **21**, 2476–2481.
45 S. Chatterjee, S. Chatterjee, B. P. Chatterjee, A. R. Das and A. K. Guha, *J. Colloid Interface Sci.*, 2005, **288**, 30–35.
46 C. Shen, Y. Shen, Y. Z. Wen, H. Y. Wang and W. P. Liu, *Water Res.*, 2011, **45**, 5200–5210.